# Role of Non-Hydrogen-Bonded Molecules in the Oxygen K-Edge Spectrum of Ice

**Tuomas Pylkkänen,*,†,‡ Valentina M. Giordano,‡ Jean-Claude Chervin,§ Arto Sakko,† Mikko Hakala,† J. Aleksi Soininen,† Keijo Hämäläinen,† Giulio Monaco,‡ and Simo Huotari‡**

*Department of Physics, P.O. Box 64, FI-00014, University of Helsinki, Finland, European Synchrotron Radiation Facility, B.P. 220, F-38043 Grenoble, France, and Physique des Milieux Condensés, IMPMC, CNRS-UMR 7590, Université Pierre et Marie Curie, F-75015 Paris, France*

*Received: December 28, 2009; Revised Manuscript Received: February 5, 2010*

We report the oxygen K-edge spectra of ices Ih, VI, VII, and VIII measured with X-ray Raman scattering. The pre-edge and main-edge contributions increase strongly with density, even though the hydrogen bond arrangements are very similar in these phases. While the near-edge spectral features in water and ice have often been linked to hydrogen bonding, we show that the spectral changes in the phases studied here can be quantitatively related to structural changes in the second coordination shell. Density-functional theory calculations reproduce the experimental results and support the conclusion. Our results suggest that non-hydrogen-bonded neighbors can have a significant effect also in the liquid water spectrum. We discuss the implications of the results for the actively debated interpretation of the liquid water spectrum in terms of local structure.

## Introduction

Liquid water, one of the most common substances and a seemingly simple system, still eludes a complete description at the molecular level. The nature and extent of hydrogen bonding in the liquid is constantly debated,[1–3] and the structural origins of its well-known anomalies are not universally agreed upon.[4] High-quality diffraction results of liquid water, which together with simulations typically point to a near-tetrahedral structure,[5] have also been modeled with a nontetrahedral model.[6,7] Furthermore, molecular dynamics simulations of water are notably sensitive to simulation parameters[8] and consequently lack full predictive power. Water is thus an important case where spectroscopic studies can contribute significantly to a more detailed understanding of the structure. One of the exceptional features of water is the large polymorphism of the crystalline phase.[9] The structurally well-characterized ice phases can act as valuable model systems for studying the connection between local structure and spectral features.

Recently, there has been a large renewed activity in the study of hydrogen bonding in liquid water and ices with X-ray spectroscopies,[1,3,10–21] in particular X-ray absorption near-edge spectroscopy (XANES)[22] and X-ray Raman scattering (XRS).[23] On the basis of the study of liquid water and ice Ih with various bulk and surface-sensitive techniques, the O K-edge XANES has been shown to be sensitive to distortion and breaking of the hydrogen bond (HB).[1,11] Liquid water XANES results have been variously interpreted either to infer significant HB asymmetry[1] or to be compatible with near-tetrahedral order,[24,25] with the choice of the theoretical method influencing the conclusions considerably.[26] Furthermore, a pioneering XRS study[16] of the high-pressure ices II, III, and IX linked pre-edge changes with differences in proton ordering. Finally, a recent study[20] including low (LDA) and high-density amorphous (HDA) ices classified the spectra into two distinct groups with either ordered (Ih, Ic, LDA) or disordered (liquid, HDA) structures. These different views highlight that there is currently no consensus of a direct relationship between structure and the near-edge spectrum, and extracting structural information from the spectra has remained controversial.

Here we extend O K-edge measurements to the high-pressure ice phases VI, VII, and VIII, which is only possible in situ with XRS utilizing hard X-rays. These ices are much denser ($\rho$ = 1.37, 1.60, 1.62 g/cm$^3$, respectively) than ice Ih (0.92 g/cm$^3$). Density increase in ice influences the bonded (first-shell) neighbors very little, whereas the nonbonded (second-shell) neighbors move significantly closer.[9] This entails at first a large bending of O−O−O angles, and at larger densities, as studied here, a transformation into crystal structures with two interpenetrating sublattices. High-pressure ices thus allow systematically examining the effect of nonbonded molecules, which have not been focused on in previous studies of the XANES of water.

In this article, we report on a large increase in the pre and main-edge features of the XANES spectra of high-pressure ices with increasing density. Similar spectral changes have been previously assigned to disorder or bond distortions in the first coordination shell. We show that our results can be instead explained as an effect of increasing coordination from approaching non-hydrogen-bonded neighbors. Density-functional theory (DFT) based spectral calculations reproduce the behavior and support the conclusion. We also discuss the implications of our findings for the interpretation of the liquid water spectrum in terms of local structure.

## Experimental Methods

Inelastic X-ray scattering experiments were performed at the beamline ID16 of the European Synchrotron Radiation Facility (ESRF).[27] The radiation was monochromatized with Si(111) and Si(440) monochromators and the beam focused to 130(H) × 50(V) $\mu$m$^2$. The scattered radiation was analyzed with bent Si(660) crystal analyzers ($R$ = 1 m) and detected with a photon-counting pixel detector. XRS spectra were collected by scanning

* To whom correspondence should be addressed. E-mail: tuomas.pylkkanen@helsinki.fi.
† University of Helsinki.
‡ European Synchrotron Radiation Facility.
§ Université Pierre et Marie Curie.

10.1021/jp912208v 
Published on Web 02/26/2010

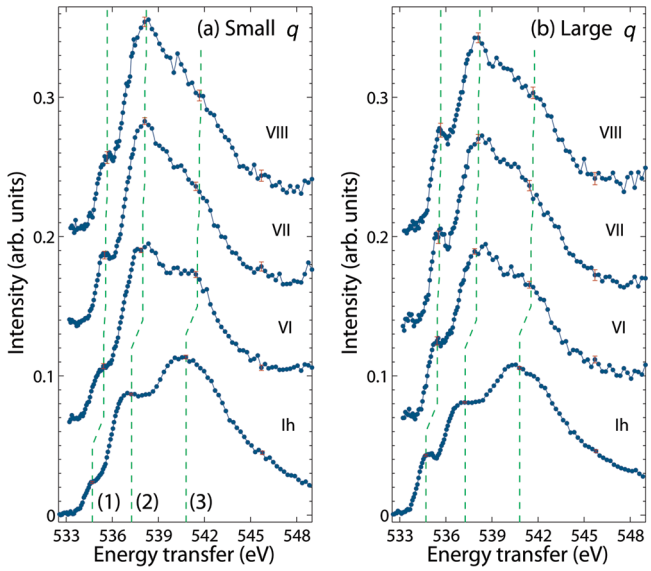


**Figure 1.** Oxygen near-K-edge spectra of ices Ih and VI−VIII. (a) XRS spectra at small momentum transfer (error bars at selected points). Lines mark (1) pre-edge, (2) main edge, and (3) post-edge positions. (b) Spectra at large momentum transfer.

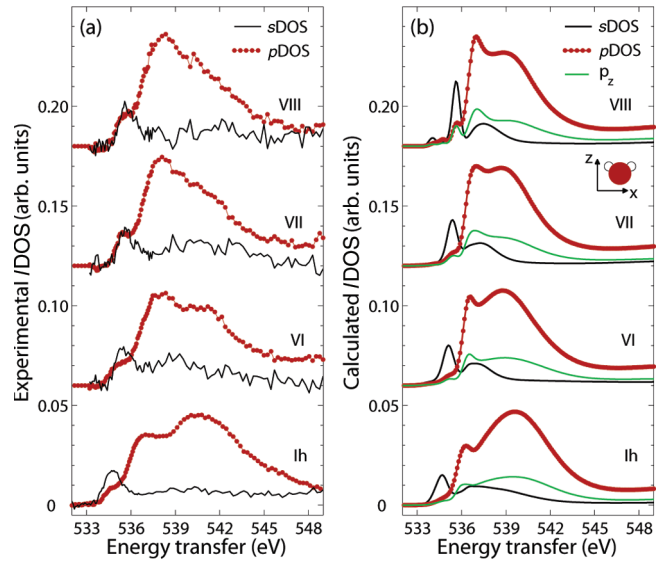


**Figure 2.** (a) Angular-momentum projections of the local density of empty states extracted from the XRS experiments. (b) DFT results of the *s*DOS and *p*DOS including the $p_z$ component (directions defined in the inset).

the incident energy while keeping the analyzer energy fixed at 9.68 keV. The total energy resolution of the setup was 0.5 eV (fwhm). Near-edge spectra were measured by scanning the energy transfer across the oxygen K-edge at 535 eV, which gives information similar to XANES (see discussion below).

High-pressure measurements were done with a panoramic diamond-anvil cell.[28,29] Ultrapure water was loaded in a Be gasket with a ruby sphere for pressure determination.[30,31] Ice VI was measured at 1.7 GPa and ices VII and VIII at 2.2 GPa with a sample size of ~300 $\mu$m along the beam. To produce ice VIII, the sample was cooled to 255 K with a cold dry-air flow. The phases were verified with in situ X-ray diffraction. All the high-pressure samples were found to be polycrystalline. For the XRS studies eight analyzers were used simultaneously. The measurements were done at two separate scattering angles of 49° and 137°, yielding momentum transfers $q = 4.2 \pm 1.2$ and $9.4 \pm 0.5$ Å$^{-1}$, respectively. The imaging properties of the bent analyzers combined with a pixel detector allowed an efficient separation of scattering from the sample and the gasket.[27] The average countrates at the main edge were 1.8 (3.7) cps per analyzer over a background of 1.9 (50) cps for $q = 4.2$ (9.4) Å$^{-1}$. A single crystal of ice Ih obtained by a modified Bridgman technique was measured at ambient pressure in a separate experiment using a cryostat at 130 K. For this measurement, six analyzer crystals were used with scattering angles of 36° and 138° ($\mathbf{q} \parallel \hat{c}$), giving $q = 3.1 \pm 0.8$ and $9.4 \pm 0.3$ Å$^{-1}$, respectively.

## Results and Discussion

The measured near-edge spectra are shown in Figure 1. The spectra are corrected for background from valence electrons[32] and normalized to have equal area in the range 533−549 eV. The main features are marked: (1) pre-edge at $E_p = 534.7$ eV (ice Ih), 535.4 eV (VI), 535.6 eV (VII), 535.7 eV (VIII); (2) main edge at $E_p + 2.6$ eV; (3) post-edge at $E_p + 6.1$ eV. We observe large changes going from ice Ih to VI and VII/VIII: the pre- and main-edge components increase, while the post-edge height remains nearly constant and the distinct post-edge peak of ice Ih disappears. There is also a small shift of the edge position into higher energies with increasing density. The proton-ordering transition between ices VII and VIII[33] does not seem to influence the spectra, which are found to be identical within the statistical accuracy. The spectra measured at small and large momentum transfers differ significantly only at the pre-edge region for all the ices studied here.

In the limit of small momentum transfer, XRS spectra are equivalent to XANES spectra and probe the *p*-type local density of empty states (DOS) at the K-edge.[23] At finite $q$, however, the XRS spectra depend on all the angular-momentum projections of DOS, denoted here generally as the *l*DOS. In the case of the oxygen K-edge in $H_2O$, only the *s*- and *p*-type DOS contribute to the spectra measurably.[34] Two measurements at sufficiently different $q$ can then be used to determine the *s*- and *p*DOS. The decomposition method[35] is based on a connection between the XRS spectra and the *l*DOS via transition matrix elements $|M_l|^2$. We use the approach that is valid for directionally averaged systems (eq 6 of ref 35). The $|M_l|^2$ are embedded atomic properties that depend weakly on the local environment and can be obtained from a real-space multiple scattering calculation with the FEFF code.[36,37] The matrix elements were calculated for each ice phase separately using the experimental $q$ values. The calculations were done on clusters with a radius of 6 Å using the Hedin−Lundqvist exchange−correlation potential. The XRS spectra were normalized to theoretical spectra in the range 533−549 eV, and the *l*DOS were extracted using least-squares matrix inversion following ref 35. A key benefit of the method is that it quantifies the contribution due to nondipole transitions in XRS.

The extracted experimental *l*DOS are shown in Figure 2a. The *p*DOS, which correspond to conventional XANES, show all the same features as the low-$q$ XRS spectra with only a slightly reduced pre-edge contribution. The *s*DOS are found to be very similar for all the ices, are dominated by a peak corresponding to the *p*DOS pre-edge position, and vary slowly after the main edge.

To gain deeper insight into the spectral fingerprints, the experimental results are compared with calculations employing Kohn−Sham (KS) DFT within the transition potential approximation.[38] The method has been useful in the interpretation of near-edge spectra of various materials.[11,39–41] DFT calculations

were performed using the StoBe-deMon code[42] and the spectra were calculated within the framework presented in ref 41. The *l*DOS were calculated using a radial representation of KS orbitals in the vicinity of the excited oxygen site. The model clusters were created on the basis of the known crystallographic structures[9,33] taking into account proton disorder.[43] Convergence with respect to cluster size was reached using 59 molecules. Calculations using the local-density approximation gave equivalent results within experimental statistics with those using a gradient-corrected functional[44,45] apart from a rigid energy shift of 5.3 eV. A Gaussian broadening scheme[1,26] was applied to the stick spectra with fwhm = 0.6 eV below 536.5 and 8.0 eV above 545 eV. Between 536.5 and 545 eV, the fwhm was linearly increased from 0.6 to 8.0 eV.

The calculated near-edge spectra are shown in Figure 2b, lined up with the experimental *s*DOS peak position with a common energy shift of −3.2 eV. The DFT results reproduce the general trends of the experiment well: a slight shift of the edge energy, a sharp *s*DOS peak at the pre-edge position (compatible with the s + $p_z$ character of the $4a_1$ LUMO orbital of an isolated $H_2O$ molecule), and a redistribution of *p*DOS weight from the post-edge to main-edge and pre-edge regions. The inclusion of proton disorder as an average over several clusters[43] broadens the spectra slightly, as is seen when ices VII and VIII are compared, but the individual ice VII spectra are very similar to the ice VIII spectrum. The calculated spectra do not completely match the experimental ones, but it is well-known that the spectral shapes obtained with this method depend strongly on, e.g., the broadening scheme used.[26]

By additionally decomposing the *p*DOS into *x*, *y*, and *z*-components (see Figure 2b for directions), our calculations identify that the observed remarkable increase in the *p*DOS pre-edge originates mainly from the $p_z$ component. Earlier, the pre-edge increase in liquid water relative to ice Ih[1] and ice III relative to IX[16] has been associated with an asymmetry in the hydrogen bonds via reduced coordination, essentially implying a dependence on the $p_x$ component. We find, however, that the *p*DOS pre-edge feature can be present even with fully coordinated molecules and symmetric bonds through the $p_z$ component.

The properties of the core-excited states are relevant also for the analysis of resonant X-ray spectra. Nordlund et al.[46] used resonant Auger-electron spectroscopy (RAES) to estimate the delocalization rate of the core-excited electron in specific final states of the X-ray absorption process in liquid water and the surface of ice Ih. They conclude that an electron excited to the pre-edge stays localized for >20 fs, whereas excitation to the post-edge results in delocalization in <0.5 fs. These time scales can be compared to the O 1s core−hole lifetime of 3.6 fs. Delocalization in RAES can be associated with excitations either into diffuse Rydberg orbitals or into the conduction band.[47] Following the procedure of ref 46, we analyzed representative final states of our static half-core−hole calculations in terms of their localization. Final states related to the pre-edge and main-edge are locally similar to monomer molecular orbitals around the excited oxygen (with $a_1$ and $b_2$ monomer symmetries, respectively) but also have significant density spread across the cluster. Post-edge-related final states are fully delocalized across the cluster. Therefore our calculations show delocalization of all the unoccupied electronic states for these ices, which is in contrast to the case of liquid water and the surface of ice, where broken bonds were seen to lead to localized pre-edge excited states.[46]

To compare the spectra more directly, we show the low-*q* XRS results of Figure 1a overlaid in Figure 3. We also include

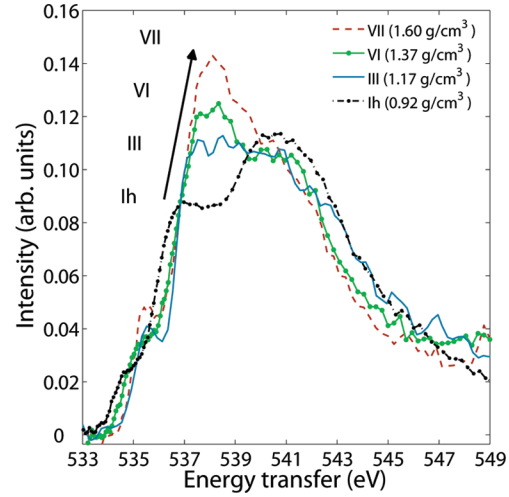


**Figure 3.** Evolution of spectral features with increasing density. For comparison, the ice III spectrum from ref 16 is convoluted to match the energy resolution in this work.

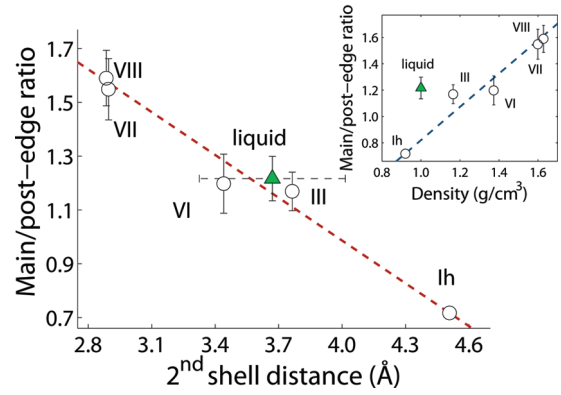


**Figure 4.** Main-to-post-edge ratio as a function of the average second-shell distance $R_{OO}^{second}$, calculated from 4 nearest nonbonded neighbors (averaged over nonequivalent central oxygen positions). Dashed line: linear fit to our results. The error bars are obtained by varying the edge positions by ±0.5 eV. For liquid water, $R_{OO}^{second}$ is taken as the average distance of the fifth to eighth nearest neighbors,[48] and the dashed horizontal error bar corresponds to the width (±$\sigma$) of this distribution. Inset: density dependence of the main-to-post-edge ratio.

the earlier XRS result of Cai et al.[16] of ice III taken at 0.25 GPa and 245 K ($\rho$ = 1.17 g/cm$^3$, intermediate between Ih and VI). It has already been seen in Figures 1 and 2 that the proton-order transition VII−VIII does not change the spectral shape. Furthermore, the hydrogen-bonded molecules' coordination changes little in these ice phases.[9] The question remains: where do the large spectral changes originate from? The most obvious difference between these phases is naturally the density. In fact, when the spectra are compared as in Figure 3, they seem to follow a systematic behavior: when the density increases, the main edge gains spectral weight while the post-edge shape changes little. The pre-edge increases in line with the main edge, although ice III has a somewhat sharper pre-edge than ice VI.

To quantify the spectral changes seen in Figure 3, we have determined the main-to-post-edge ratio of these ices on the basis of the positions shown in Figure 1 (for ice III, we use $E_p$ = 535.5 eV). The result is presented in Figure 4 inset as a function of density and is seen to follow a nearly linear behavior. However, it should be emphasized that since the first coordination shell is similar in all these systems, the density differences actually reflect the approach of the outer, non-hydrogen-bonded, molecules. Indeed, the O−O distance varies very little between

these phases, from 2.76 Å (ice Ih) to 2.77 Å (III, VI) and 2.90 Å (VII, VIII).[9,33] However, the second-shell distance $R_{OO}^{second}$ changes markedly from 4.51 Å (Ih) to 3.76 Å (III), 3.44 Å (VI), and 2.89 Å (VII, VIII), with the nonbonded neighbors finally coming even closer than the hydrogen-bonded ones. Figure 4 shows how the main-to-post-edge ratio is clearly correlated with the second-shell distance.

Interestingly, Fister et al.[49] recently found a similar behavior in the intermediate energy range (~10−50 eV above the edge) fine structure of ice. On the basis of XRS experiments on ice Ih and real-space full-multiple-scattering calculations (RSFMS) of various ice phases, the spectra were found to be sensitive to the intermediate-range local order (up to ~7 Å from the absorbing atom) in this energy range. However, as pointed out by the authors, RSFMS calculations using spherical muffin-tin potentials may fail in the very near-edge region (within ~10 eV of the edge). Here we use molecular-orbital-based calculations to confirm the effect of nonbonded neighbors on the near-edge spectra. Medium-range-order has also been shown to have an important effect in the metal K-edge XANES of transition metal oxides,[50,51] where the use of new spectroscopic tools such as resonant X-ray emission[52,53] can reveal structure normally hidden by the core-hole lifetime broadening.

To demonstrate that density increase alone does not explain the spectral changes, we have also performed calculations using a model structure of dense ice, obtained by scaling the O−O distances in ice Ih while keeping the intramolecular structure intact. Such a model produced spectra with an increasing post-edge as a function of density, in disagreement with the experimental result of Figure 3, while the calculations using the proper structures (Figure 2b) show the correct behavior. Since $R_{OO}^{second}$ is the only physically meaningful variable that changes systematically between these phases and scales with the spectral weight ratio, the spectra can be concluded to directly reflect the changes in $R_{OO}^{second}$. This result is remarkable since it essentially gives a fingerprint of the second-shell structure based on a clearly observable shape of the XANES spectrum in cases where the first-shell structure is known. Importantly, our main conclusion can be drawn solely from experimental data and provides a benchmark for any future spectral calculations of water and ice, which should explicitly consider the influence of nonbonded neighbors.

We next consider the relevance of our results for the interpretation of the liquid water XANES spectrum. As reported by various authors,[1,15,16,20] the liquid water spectrum deviates strongly from that of ice Ih and is characterized by pronounced pre- and main-edge components, similar to the spectrum of ice VI shown here. To make the connection to the present work, we extracted the main-to-post-edge ratio of liquid water from the XRS data of Tse et al.[20] (using $E_p = 535.0$ eV) and include it in Figure 4 as a separate point. Although the density of liquid water is near that of ice Ih (1.0 vs 0.92 g/cm$^3$), the main-to-post-edge ratio is closer to that of ices III and VI, as shown in the Figure 4 inset. The large spectral change between ice Ih and liquid water has been previously attributed to distortion and breaking of hydrogen bonds,[1,15,16] or to increased disorder in the HB network.[20] Our results show that increased coordination is an important factor that has not been previously considered.

The second-shell distance in liquid water has a broad distribution, ranging from the outer part of the first coordination shell up to the tetrahedral second-neighbor distance of ice Ih. Increased coordination is apparent from the O−O coordination number, which is 4.4−4.7 for liquid water,[5,54,55] compared to 4.0 for ice Ih. The average distance of the nearest second-shell molecules (fifth to eighth instantaneous neighbors) was $\langle R_{OO}^{second} \rangle = 3.7 \pm 0.3$ Å in a molecular dynamics simulation using the TIP4P model.[48] In another simulation using the TIP5P model, the average distance of the closest second-shell molecule (fifth neighbor) was 3.5 Å.[56] Interpreting the above average distance $\langle R_{OO}^{second} \rangle$ as the equivalent $R_{OO}^{second}$ value for the liquid, we find that water also tentatively fits the correlation reported in Figure 4.

The amorphous ices show a similar behavior: HDA ice ($\rho = 1.17$ g/cm$^3$) has a coordination number of $5.0 \pm 0.1$,[57] in contrast with the value $3.9 \pm 0.1$ for LDA ice ($\rho = 0.94$ g/cm$^3$). The second-shell peak in the O−O partial radial distribution function of LDA ice (at 4.5 Å) splits in HDA ice and significant weight is added around ~3.6 Å.[57] The near-edge spectra of LDA and ice Ih are nearly identical, as are the HDA and liquid water spectra.[20] Our results suggest that the spectral changes in the amorphous ices can also be related to increased coordination.

We note that the disordered first coordination shell of liquid water is naturally different from those of the ices, and the correlation of Figure 4 was derived considering only structures with similar first coordination shells. Detailed computational studies should be performed to confirm the influence of nonbonded molecules in the liquid water spectrum. Nevertheless, it is clear from our results, and the similarity of the water spectrum to those of high-pressure ices, that increased coordination from the nonbonded neighbors can play an important role also in the liquid water spectrum.

## Conclusions

We find a new behavior in the oxygen near-edge spectra of water ices: even in the presence of fully coordinated molecules, strong pre-edge and main-edge changes can be produced by increased density via an approaching second coordination shell. Similar changes have previously been related to broken hydrogen bonds,[1] proton disorder,[16] or increased disorder in the HB network.[20] Our findings show that such spectral fingerprints can also be induced by increased coordination, without breaking bonds (as all the ices studied here have similar bonds) and without increasing disorder, which is clear from the similarity of the spectra of the proton-disordered ice VII and proton-ordered ice VIII. Our findings may have implications on the much-debated interpretation of the XANES spectrum of liquid water, where the influence of increased coordination from non-hydrogen-bonded neighbors should definitely be taken into account.

**Acknowledgment.** We thank Juliette Chevy (Laboratoire de Glaciologie et Géophysique de l'Environnement, CNRS, Grenoble) for providing the ice Ih sample. This work has been supported by the Academy of Finland, Contract No. 110571, and its Centers of Excellence Program (2006-2011). J.A.S. acknowledges funding by the Magnus Ehrnrooth Foundation.

## References and Notes

(1) Wernet, Ph.; Nordlund, D.; Bergmann, U.; Cavalleri, M.; Odelius, M.; Ogasawara, H.; Näslund, L. Å.; Hirsch, T. K.; Ojamäe, L.; Glatzel, P.; Pettersson, L. G. M.; Nilsson, A. *Science* **2004**, *304*, 995–999.

(2) Head-Gordon, T.; Johnson, M. E. *Proc. Natl. Acad. Sci. U.S.A.* **2006**, *103*, 7973–7977.

(3) Huang, C.; et al. *Proc. Natl. Acad. Sci. U.S.A.* **2009**, *106*, 15214–15218.

(4) Ball, P. *Nature* **2008**, *452*, 291–292.

(5) Head-Gordon, T.; Hura, G. *Chem. Rev.* **2002**, *102*, 2651–2670.

(6) Soper, A. K. *J. Phys.: Condens. Matter* **2005**, *17*, S3273–S3282.

(7) Leetmaa, M.; Wikfeldt, K. T.; Ljungberg, M. P.; Odelius, M.; Swenson, J.; Nilsson, A.; Pettersson, L. G. M. *J. Chem. Phys.* **2008**, *129*, 084502.

(8) Guillot, B. *J. Mol. Liq.* **2002**, *101*, 219–260.
(9) Petrenko, V. F.; Whitworth, R. W. *Physics of Ice*; Oxford University Press: Oxford, U.K., 1999.
(10) Bowron, D. T.; Krisch, M. H.; Barnes, A. C.; Finney, J. L.; Kaprolat, A.; Lorenzen, M. *Phys. Rev. B* **2000**, *62*, R9223–R9227.
(11) Myneni, S.; Luo, Y.; Näslund, L. Å.; Cavalleri, M.; Ojamäe, L.; Ogasarawa, H.; Pelmenschikov, A.; Wernet, Ph.; Västerlein, Z.; Pettersson, L. G. M.; Nilsson, A. *J. Phys.: Condens. Matter* **2002**, *14*, L213–L219.
(12) Bergmann, U.; Wernet, Ph.; Glatzel, P.; Cavalleri, M.; Pettersson, L. G. M.; Nilsson, A.; Cramer, S. P. *Phys. Rev. B* **2002**, *66*, 092107.
(13) Guo, J.-H.; Luo, Y.; Augustsson, A.; Rubensson, J.-E.; Såthe, C.; Ågren, H.; Siegbahn, H.; Nordgren, J. *Phys. Rev. Lett.* **2002**, *89*, 137402.
(14) Parent, P.; Laffon, C.; Mangeney, C.; Bournel, F.; Tronc, M. *J. Chem. Phys.* **2002**, *117*, 10842.
(15) Smith, J. D.; Cappa, C. D.; Wilson, K. R.; Messer, B. M.; Cohen, R. C.; Saykally, R. J. *Science* **2004**, *306*, 851–853.
(16) Cai, Y. Q.; et al. *Phys. Rev. Lett.* **2005**, *94*, 025502.
(17) Odelius, M.; Ogasawara, H.; Nordlund, D.; Fuchs, O.; Weinhardt, L.; Maier, F.; Umbach, E.; Heske, C.; Zubavichus, Y.; Grunze, M.; Denlinger, J. D.; Pettersson, L. G. M.; Nilsson, A. *Phys. Rev. Lett.* **2005**, *94*, 227401.
(18) Mao, W. L.; Mao, H.-K.; Meng, Y.; Eng, P. J.; Hu, M. Y.; Chow, P.; Cai, Y. Q.; Shu, J.; Hemley, R. J. *Science* **2006**, *314*, 636–638.
(19) Fukui, H.; Huotari, S.; Andrault, D.; Kawamoto, T. *J. Chem. Phys.* **2007**, *127*, 134502.
(20) Tse, J. S.; Shaw, D. M.; Klug, D. D.; Patchkovskii, S.; Vankó, G.; Monaco, G.; Krisch, M. *Phys. Rev. Lett.* **2008**, *100*, 095502.
(21) Fuchs, O.; Zharnikov, M.; Weinhardt, L.; Blum, M.; Weigand, M.; Zubavichus, Y.; Bär, M.; Maier, F.; Denlinger, J. D.; Heske, C.; Grunze, M.; Umbach, E. *Phys. Rev. Lett.* **2008**, *100*, 027801.
(22) Stöhr, J. *NEXAFS Spectroscopy*; Springer-Verlag: Berlin, 1992.
(23) Schülke, W. *Electron Dynamics by Inelastic X-Ray Scattering*; Oxford University Press,: Oxford, U.K., 2007.
(24) Hetényi, B.; Angelis, F. D.; Giannozzi, P.; Car, R. *J. Chem. Phys.* **2004**, *120*, 8632–8637.
(25) Prendergast, D.; Galli, G. *Phys. Rev. Lett.* **2006**, *96*, 215502.
(26) Smith, J. D.; Cappa, C. D.; Messer, B. M.; Drisdell, W. S.; Cohen, R. C.; Saykally, R. J. *J. Phys. Chem. B* **2006**, *110*, 20038–20045.
(27) Verbeni, R.; Pylkkänen, T.; Huotari, S.; Simonelli, L.; Vankó, G.; Martel, K.; Henriquet, C.; Monaco, G. *J. Synchrotron Rad.* **2009**, *16*, 469–476.
(28) Mao, H. K. *Science* **2001**, *292*, 914–916.
(29) Chervin, J. C.; Feret, H.; Rey, N.; Poloni, R.; Machon, D.; Le Floch, S.; San Miguel, A. PanoramiX: a diamond anvil cell designed for radial X-ray investigations. *Proceedings of the 5e Forum de technologie des hautes pressions*, 2006.
(30) Mao, H. K.; Bell, P. M.; Shaner, J. W.; Steinberg, D. J. *J. Appl. Phys.* **1978**, *49*, 3276–3283.
(31) Chervin, J. C.; Canny, B.; Mancinelli, M. *High Pressure Res.* **2001**, *21*, 305–314.
(32) The background consists of inelastic scattering from the valence electrons (Compton scattering in the case of large momentum transfer). A linear background was subtracted from the low-$q$ spectra. For the large-$q$ spectra, a phenomenological background function (Pearson VII[58]) was fitted to each analyzer signal in the energy range 400−530 eV. Such an approach allowed a very accurate background removal for the first ∼20 eV near the edge. For the extended energy range fine structure, a detailed analysis incorporating a model of the Compton profile is crucial.[59]
(33) Kuhs, W. F.; Finney, J. L.; Vettier, C.; Bliss, D. V. *J. Chem. Phys.* **1984**, *81*, 3612–3623.
(34) For near-edge XRS from 1s initial states, d-type final states are effectively unobservable for practically accessible values of $q$.[60,61] In our FEFF calculations, the d-contribution is less than 0.5% at the O K-edge for $q < 10$ Å$^{-1}$.
(35) Soininen, J. A.; Mattila, A.; Rehr, J. J.; Galambosi, S.; Hämäläinen, K. *J. Phys.: Condens. Matter* **2006**, *18*, 7327–7336.
(36) Ankudinov, A. L.; Ravel, B.; Rehr, J. J.; Conradson, S. D. *Phys. Rev. B* **1998**, *58*, 7565–7576.
(37) Soininen, J. A.; Ankudinov, A. L.; Rehr, J. J. *Phys. Rev. B* **2005**, *72*, 045136.
(38) Triguero, L.; Pettersson, L. G. M.; Ågren, H. *Phys. Rev. B* **1998**, *58*, 8097–8110.
(39) Nyberg, M.; Odelius, M.; Nilsson, A.; Pettersson, L. G. M. *J. Chem. Phys.* **2003**, *119*, 12577–12585.
(40) Wilson, K. R.; Cavalleri, M.; Rude, B. S.; Schaller, R. D.; Catalano, T.; Nilsson, A.; Saykally, R. J.; Pettersson, L. G. M. *J. Phys. Chem. B* **2005**, *109*, 10194–10203.
(41) Sakko, A.; Hakala, M.; Soininen, J. A.; Hämäläinen, K. *Phys. Rev. B* **2007**, *76*, 205115.
(42) Hermann, K.; Pettersson, L. G. M.; Casida, M. E.; Daul, C.; Goursot, A.; Koester, A.; Proynov, E.; St-Amant, A.; Salahub, D. R. *Stobe-demon version 3.0*, 2007.
(43) For the proton-disordered ices Ih, VI, and VII, random proton configurations were created that assign H occupations while satisfying the Bernal−Fowler ice rules and producing minimal total dipole moment. Twenty clusters with different proton configurations were used for each phase and the results averaged, while only one cluster was used for the fully ordered ice VIII. The intramolecular structure was fixed following refs 9 (ice Ih), 62 (VI), and 63 (VII). For ice VI, central molecules belonging to both crystallographic nonequivalent oxygen positions 2a and 8g were used and the result is a weighted average.
(44) Becke, A. D. *Phys. Rev. A* **1988**, *38*, 3098–3100.
(45) Perdew, J. P. *Phys. Rev. B* **1986**, *33*, 8822–8824.
(46) Nordlund, D.; Ogasawara, H.; Bluhm, H.; Takahashi, O.; Odelius, M.; Nagasono, M.; Pettersson, L. G. M.; Nilsson, A. *Phys. Rev. Lett.* **2007**, *99*, 217406.
(47) Winter, B.; Hergenhahn, U.; Faubel, M.; Björneholm, O.; Hertel, I. V. *J. Chem. Phys.* **2007**, *127*, 094501.
(48) Saitta, A. M.; Datchi, F. *Phys. Rev. E* **2003**, *67*, 020201.
(49) Fister, T. T.; Nagle, K. P.; Vila, F. D.; Seidler, G. T.; Hamner, C.; Cross, J. O.; Rehr, J. J. *Phys. Rev. B* **2009**, *79*, 174117.
(50) Wu, Z. Y.; Xian, D. C.; Hu, T. D.; Xie, Y. N.; Tao, Y.; Natoli, C. R.; Paris, E.; Marcelli, A. *Phys. Rev. B* **2004**, *70*, 033104.
(51) Gougoussis, C.; Calandra, M.; Seitsonen, A.; Brouder, C.; Shukla, A.; Mauri, F. *Phys. Rev. B* **2009**, *79*, 045118.
(52) Vankó, G.; de Groot, F. M. F.; Huotari, S.; Cava, R. J.; Lorenz, T.; Reuther, M. Intersite 4p−3d hybridization in cobalt oxides: a resonant X-ray emission spectroscopy study. 2008, arXiv: 0802.2744. arXiv.org e-Print archive. http://arxiv.org/abs/0802.2744v1 (accessed January 30, 2010).
(53) de Groot, F.; Vankó, G.; Glatzel, P. *J. Phys.: Condens. Matter* **2009**, *21*, 104207.
(54) Bergmann, U.; Di Cicco, A.; Wernet, Ph.; Principi, E.; Glatzel, P.; Nilsson, A. *J. Chem. Phys.* **2007**, *127*, 174504.
(55) Wikfeldt, K. T.; Leetmaa, M.; Ljungberg, M. P.; Nilsson, A.; Pettersson, L. G. M. *J. Phys. Chem. B* **2009**, *113*, 6246–6255.
(56) Yan, Z.; Buldyrev, S. V.; Kumar, P.; Giovambattista, N.; Debenedetti, P. G.; Stanley, H. E. *Phys. Rev. E* **2007**, *76*, 051201.
(57) Finney, J. L.; Hallbrucker, A.; Kohl, I.; Soper, A. K.; Bowron, D. T. *Phys. Rev. Lett.* **2002**, *88*, 225503.
(58) Wang, H.; Zhou, J. *J. Appl. Crystallogr.* **2005**, *38*, 830–832.
(59) Sternemann, H.; Sternemann, C.; Seidler, G. T.; Fister, T. T.; Sakko, A.; Tolan, M. *J. Synchrotron Rad.* **2008**, *15*, 162–169.
(60) Doniach, S.; Platzman, P. M.; Yue, J. T. *Phys. Rev. B* **1971**, *4*, 3345–3350.
(61) Nagle, K. P.; Seidler, G. T.; Shirley, E. L.; Fister, T. T.; Bradley, J. A.; Brown, F. C. *Phys. Rev. B* **2009**, *80*, 045105.
(62) Kuo, J.-L.; Kuhs, W. F. *J. Phys. Chem. B* **2006**, *110*, 3697–3703.
(63) Kuo, J.-L.; Klein, M. L. *J. Phys. Chem. B* **2004**, *108*, 19634–19639.

JP912208V